

[The garnet effect on hafnium isotope compositions of granitoids during crustal anatexis]

[Long Chen^{1,2,3*}, Chris Yakymchuk⁴, Kai Zhao², Zifu Zhao^{2,3,5*}, Dongyong Li¹, Peng Gao⁶, Yixiang Chen^{2,3}, Guochao Sun², Zhibin Liu²]

[¹Frontiers Science Center for Deep Ocean Multispheres and Earth System, Key Lab of Submarine Geosciences and Prospecting Techniques, MOE and College of Marine Geosciences, Ocean University of China, Qingdao 266100, China

²CAS Key Laboratory of Crust-Mantle Materials and Environments, University of Science and Technology of China, Hefei 230026, China

³Center of Excellence for Comparative Planetology, Chinese Academy of Sciences, Hefei 230026, China

⁴Department of Earth and Environmental Sciences, University of Waterloo, Waterloo, Ontario N2L 3G1, Canada

⁵Frontiers Science Center for Planetary Exploration and Emerging Technologies, University of Science and Technology of China, Hefei 230026, China

⁶School of Earth Science and Geological Engineering, Sun Yat-sen University, Guangzhou 510275, China]

*Corresponding author: E-mail: chenlong@ouc.edu.cn; zfzhao@ustc.edu.cn.

Contents of this file

Part I: Sample descriptions

Part II: Analytical methods

Part III: Figures S1-S6

Part IV: Details for quantitative simulation

Part V: Captions for supplemental tables S1-S12

Introduction

[Details about the petrography of the early-stage rocks from the Dabie orogen, analytical methods, the procedures, rationale for parameters selection, data sources as well as potential uncertainties for the quantitative modeling, as well as six supporting figures (Figures S1-S6) are listed here. Data used in these figures and figures in the main text are listed in the supplemental Tables S1-S12.]

Part I: Sample descriptions

1.1 Liangshan pluton:

Granitoids from this pluton exhibit porphyritic texture with 20-30 vol.% of phenocrysts that are mainly composed of euhedral to subhedral plagioclase and K-feldspar. The matrix is composed of plagioclase, quartz, biotite, amphibole, and titanite (Fig. S1A).

1.2 Shangcheng pluton:

Granitoids from this pluton exhibit porphyritic texture with 20-30 vol.% of phenocrysts that are dominant by euhedral to subhedral K-feldspar. The matrix is composed of plagioclase, K-feldspar, quartz, biotite, and amphibole (Fig. S1B).

1.3 Sanjiaoshan pluton:

Granitoids from this pluton are partially foliated with a weakly deformed texture. They are composed of plagioclase (30-40 vol.%), quartz (25-40 vol.%), K-feldspar (25 vol.%), biotite (3 vol.%), amphibole (2 vol.%), and small amounts of titanite and zircon (Fig. S1C).

1.4 Tiantangzhai pluton:

Granitoids from this pluton exhibit equigranular texture, with mineral grain size ranging from 0.5 to 1 mm, they are dominant by K-feldspar (40-50 vol.%) and

quartz (35-45 vol.%) with subordinate biotite (5-8 vol.%), amphibole (≤ 2 vol.%), titanite and zircon (Fig. S1D).

1.5 Egongbao pluton:

Granitoids from this pluton exhibit equigranular texture, with mineral grain sizes ranging from 0.5 to 1.5 mm, they are composed of plagioclase (30-40 vol.%), K-feldspar (20 vol.%), quartz (15-40 vol.%), amphibole (10 vol.%), biotite (8 vol.%), titanite and zircon (Fig. S1E).

1.6 Fuziling pluton:

Granitoids from this pluton exhibit equigranular texture, with mineral grain size ranging from 0.5 to 1 mm, they are dominant by plagioclase (45 vol.%), quartz (30 vol.%) and K-feldspar (20 vol.%) with subordinate amphibole (≤ 5 vol.%), biotite (≤ 5 vol.%) and accessory minerals (Fig. S1F).

1.7 Fenliupu pluton:

Granitoids from this pluton exhibit equigranular texture, with a mineral grain size of ~ 0.5 mm, they are composed of quartz (50 vol.%), plagioclase (30 vol.%), K-feldspar (15 vol.%), amphibole (≤ 5 vol.%) and biotite (Fig. S1G).

1.8 Lidian pluton:

Granitoids from this pluton are biotite-granite with weak deformation. They are composed of quartz (30 vol.%), plagioclase (30 vol.%), K-feldspar (15 vol.%), biotite (15 vol.%), amphibole (≤ 5 vol.%), and accessory apatite and zircon (Fig. S1H).

1.9 Datong pluton:

Granitoids from this pluton exhibit equigranular texture with weak deformation, they are composed of quartz (35-45 vol.%), K-feldspar (25-30 vol.%), plagioclase (20-25 vol.%), biotite (5-8 vol.%), amphibole (≤ 5 vol.%) and

accessory minerals (Fig. S1I).

1.10 Zhangbang pluton:

Granitoids from this pluton exhibit unequigranular texture, with mineral grain sizes ranging from 0.3 to 5 mm, they are composed of plagioclase (35-40 vol.%), quartz (25-35 vol.%), K-feldspar (15-20 vol.%), amphibole (8-10 vol.%), biotite (5-8 vol.%) and accessory minerals (Fig. S1J).

Part II: Analytical methods

Fresh specimens were sawed into slices and the central parts were selected to crush into powders of ~200 mesh using the agate mortar. Zircon grains were separated by the conventional magnetic and heavy liquid techniques and hand-picked using a binocular microscope. Representative zircon grains were mounted in epoxy resin and polished to expose the grain centers. Transmitted and reflected light micrographs, as well as cathodoluminescence (CL), were taken to reveal their external morphology and internal structure, which then were used as guides to the selection of in-situ analysis spots.

2.1 Zircon U-Pb ages

In-situ zircon U-Pb isotopes analyses were conducted on an Agilent 7500a ICP-MS equipped with a 193 nm ComPex102-ArF laser-ablation system, which is housed at the School of Resources and Environmental Engineering in Hefei University of Technology, Hefei. Helium (He) was used as the carrier gas, and the beam diameter of 32 μm with a repetition rate of 6 Hz was applied to all analyses with a 10 J/cm² energy density. Each analysis incorporated a background acquisition of approximately 25 s (gas blank) followed by ~60 s of data acquisition from the sample. The zircon standard Mud Tank was analyzed to monitor the accuracy of the unknown zircon age. NIST 610 was used as the external reference to normalize U, Th and Pb contents of unknowns. Zircon

91500 was used as an external standard for calibrating mass bias, elemental fractionation, and stability of the equipment during our analyses. Detailed procedures of laser analysis and data processing, as well as reference samples, are essentially the same as those used in the Xi'an laboratory ([Yuan et al., 2004](#); [Zong et al., 2010](#)).

2.2 Whole-rock major and trace elements

Whole-rock major and trace elements were analyzed at the ALS Chemex Company in Guangzhou, China. An ignited sample (~0.9 g) was mixed well with ~9.0 g lithium borate flux (50%-50% $\text{Li}_2\text{B}_4\text{O}_7$ - LiBO_2) and then fused in an auto fluxer under the temperature of 1050°C to 1100°C. The resulted melt was made into a flat molten glass disc, which was then analyzed using X-ray fluorescence spectrometry (XRF) for major elements with an analysis precision better than ± 1 -2%. For trace element analysis, a prepared sample (~0.2 g) was mixed well with lithium metaborate flux (~0.9 g) and then fused in a furnace at 1000°C to obtain the homogeneous melt, which then cooled and dissolved in 100 ml 4% nitric acid before analysis using inductively coupled plasma-mass spectrometry (ICP-MS). The analytical precision is better than $\pm 5\%$ for most trace elements.

2.3 Whole-rock Sr-Nd-Hf isotopes

Chemical separation before Sr-Nd-Hf isotopic analyses was undertaken by conventional ion-exchange techniques at State Key Laboratory of Lithospheric Evolution in IGG, CAS, Beijing. The detailed procedure is described by [Yang et al. \(2010\)](#), and only a brief introduction is given here. All chemical preparations were conducted on special class 100 workbenches inside a class 1000 clean laboratory. About 1200 mg fine sample powder was dissolved in a steel-jacketed Teflon bomb with 2.5 ml concentrated HF, 0.2 ml HNO_3 and HClO_4 , which was placed in an oven at 190 °C for one week. After complete dissolution, each sample was dried down at high temperature (fuming HClO_4) on a hot plate, then the mixture was treated with 14 M HNO_3 , evaporated to dryness overnight,

and taken up in 3 M HNO₃ + 3% m/v H₃BO₃. The capsule was resealed and placed on a hot plate at 100 °C overnight in preparation for chemical purification. Hf was firstly leached from the solution using the Ln Spec resin (modified after Münker et al., 2001) and then Sr was separated from the remaining solution using a quartz column packed with AG50W-X12. Finally, the separation of Nd was achieved using another commercial Ln Spec resin column (modified after Pin and Santos-Zalduegui, 1997).

After separation, the Sr-Nd-Hf isotopic analyses were carried out on a Neptune MC-ICP-MS at the State Key Laboratory of Lithospheric Evolution in IGG, CAS, Beijing. Details on the analytical techniques for Sr-Nd-Hf isotope were given in Wu et al. (2006) and Yang et al. (2009). Parent/daughter ratios for the above isotope couples (Rb-Sr, Sm-Nd and Lu-Hf) were determined by the solution ICP-MS method with an analytical precision better than ±5% for these elements, which is precise enough for age corrections.

The decay constants used for age calculations are: $\lambda (^{87}\text{Rb}) = 1.393 \times 10^{-11} \text{ y}^{-1}$ (Nebel et al., 2011), $\lambda (^{147}\text{Sm}) = 6.54 \times 10^{-12} \text{ y}^{-1}$ (Lugmair and Marti, 1978) and $\lambda (^{176}\text{Lu}) = 1.865 \times 10^{-11} \text{ y}^{-1}$ (Scherer et al., 2001). Initial $^{143}\text{Nd}/^{144}\text{Nd}$ and $^{176}\text{Hf}/^{177}\text{Hf}$ ratios were calculated with reference to the chondritic reservoir (CHUR) of Bouvier et al. (2008) at the time of magma solidification and denoted in the $\epsilon_{\text{Nd}}(t)$ and $\epsilon_{\text{Hf}}(t)$ notation, respectively.

Part III: Figures S1-S6

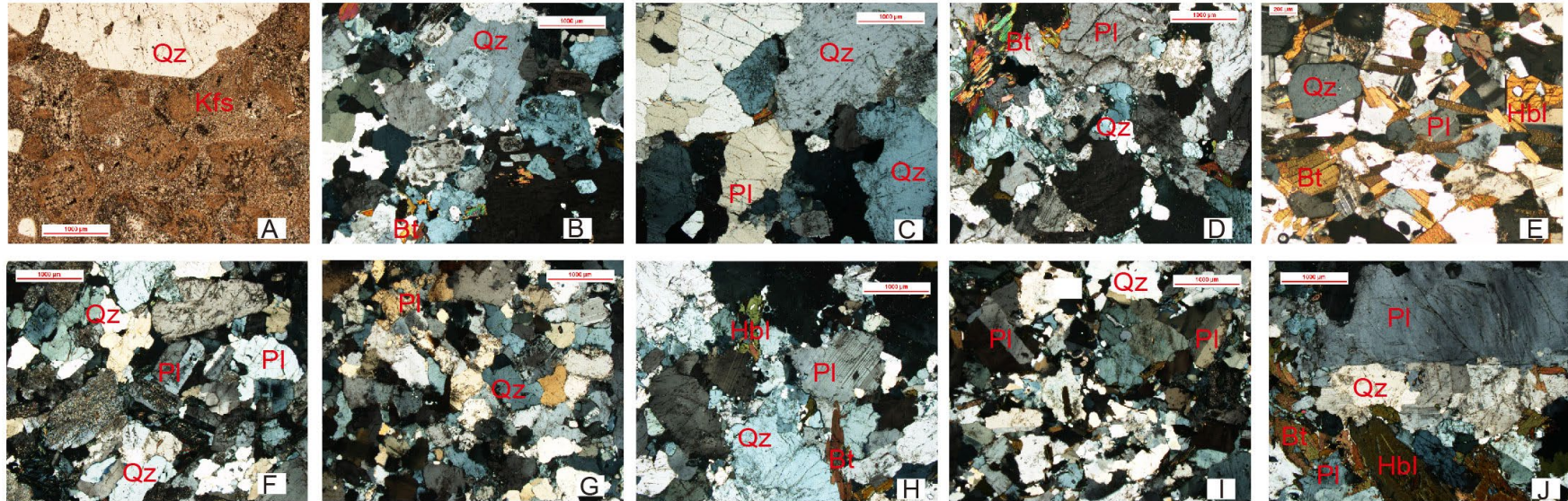


Figure S1. Petrographic microscope photographs for the post-collisional early-stage granitoids from the Dabie orogen. Panels: (A) Liangshan pluton: K-feldspar granite (15DB003); (B) Shangcheng pluton: Granite (15DB020); (C) Sanjiaoshan pluton: Gneissic granite (15DB052); (D) Tiantangzhai pluton: Granite (15DB064); (E) Egongbao pluton: Monzogranite (15DB068); (F) Fuziling pluton: Monzogranite (15DB105); (G) Fenliupu pluton: Granodiorite (15DB113); (H) Lidian pluton: Granite (15DB122); (I) Datong pluton: Granite (15DB136); (J) Zhangbang pluton: Granite (15DB141). Abbreviations: Qz-quartz; Kfs-K-feldspar; Pl-plagioclase; Bt-biotite; Hbl-hornblende.

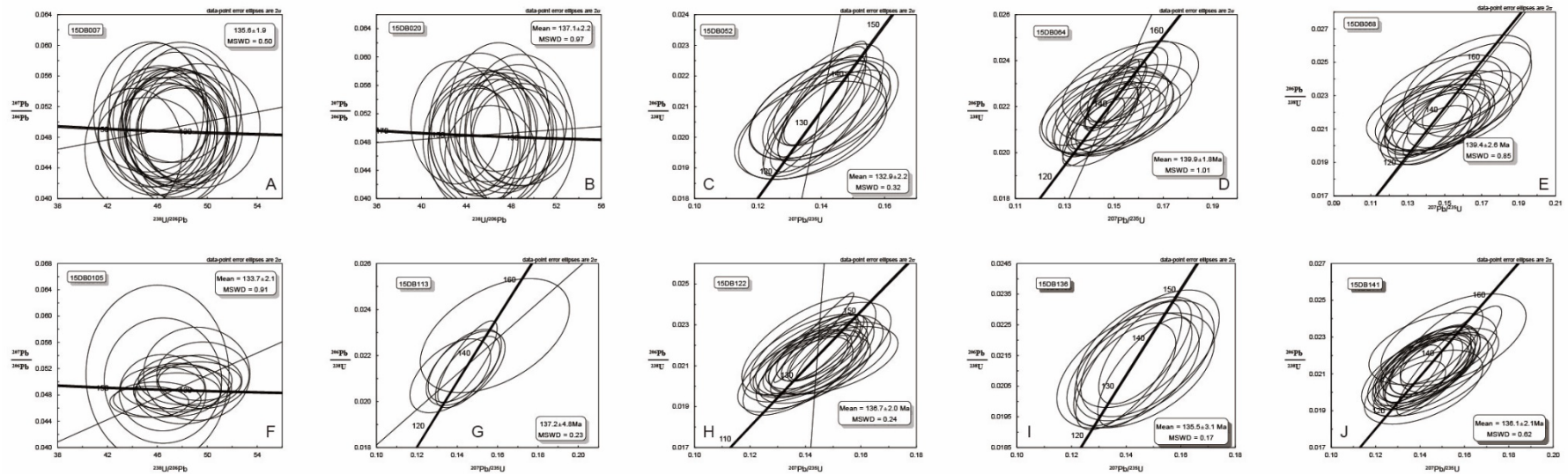


Figure S2. Concordia diagrams of zircon U-Pb isotope data analyzed by the LA-ICPMS technique for one Cretaceous early-stage granitoid sample from each pluton in the Dabie orogen. A-J, Liangshan pluton, Shangcheng pluton, Shanjiaoshan pluton, Tiantangzhai pluton, Egongbao pluton, Fuziling pluton, Fenliupu pluton, Lidian pluton, Datong pluton, and Zhangbang pluton, respectively. For the concise of the figures, relict zircons with dominantly Neoproterozoic and Triassic, and subordinate Archean and Paleo-Proterozoic U-Pb ages as listed in [Table S1](#) were not plotted.

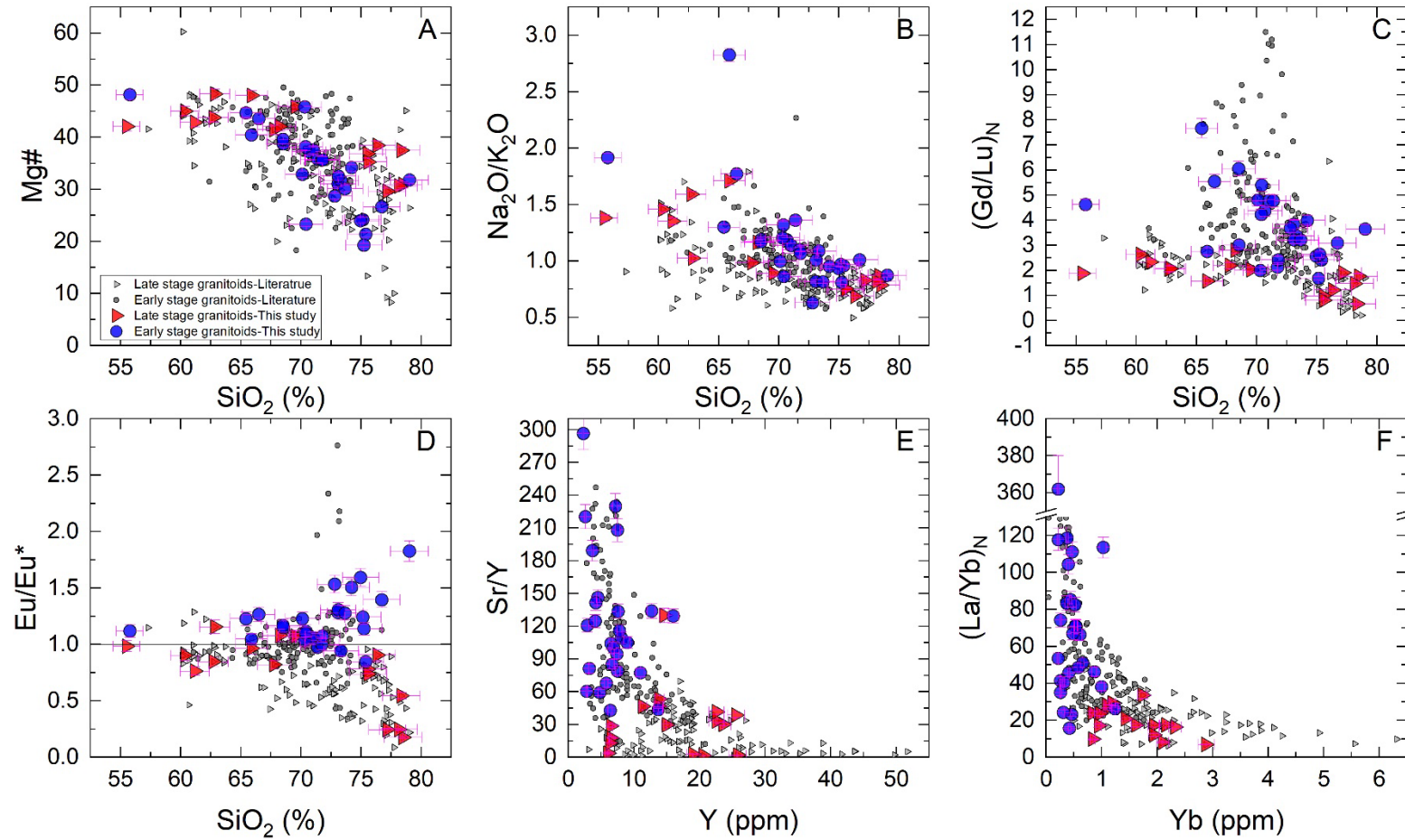


Figure S3. Whole-rock major-trace element compositions of the post-collisional early-stage and late-stage granitoids from the Dabie orogen, published data (Zhao et al., 2017) are also plotted for comparison. Uncertainties are plotted at 2σ and are smaller than the symbols when not shown. Note the large ranges of our data that are comparable to those of all the published data.

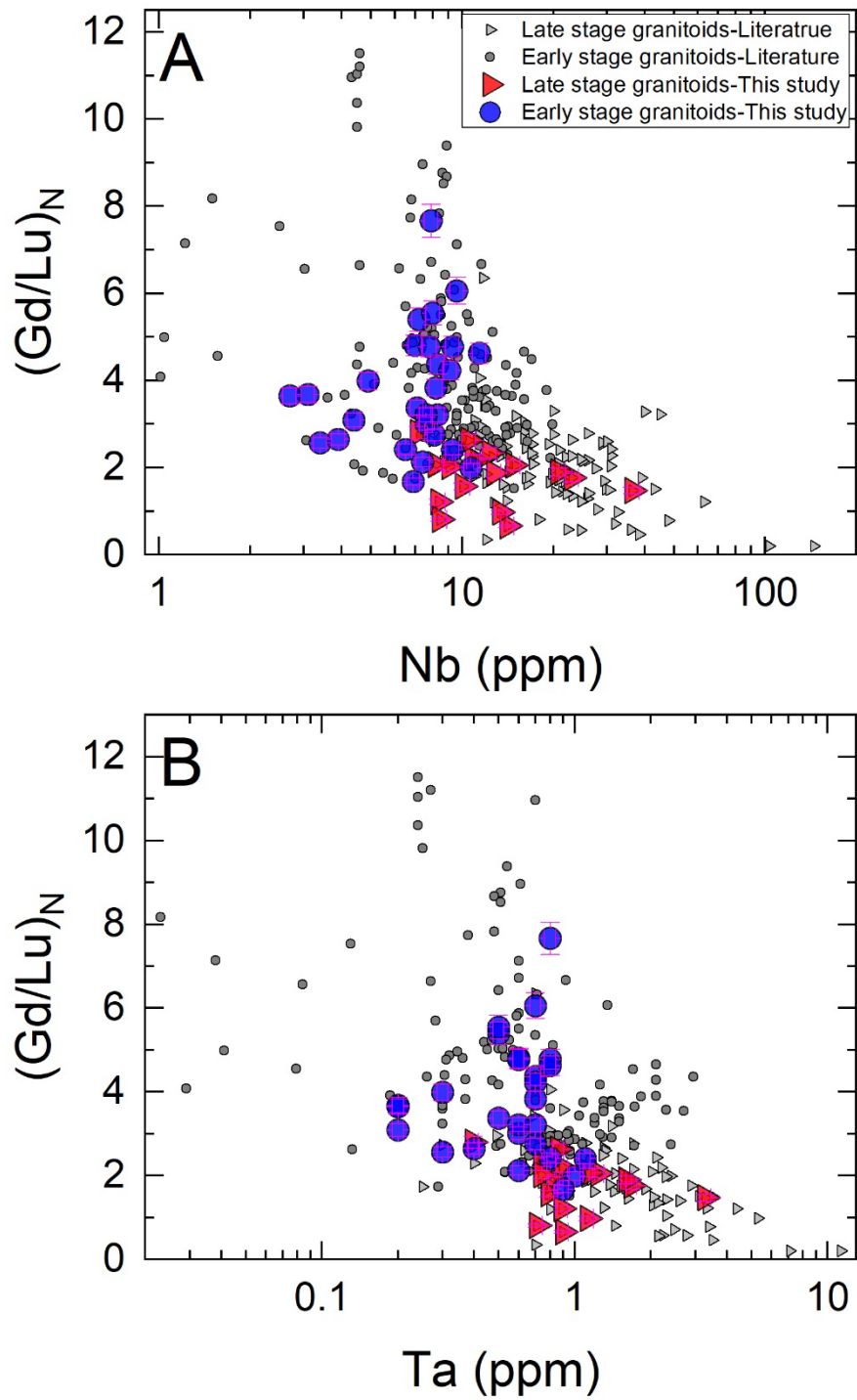


Figure S4. Plots of Nb (A) and Ta (B) versus (Gd/Lu)_N ratios for the post-collisional early-stage and late-stage granitoids from the Dabie orogen, published data (Zhao et al., 2017) are also plotted for comparison. Uncertainties are plotted at 2 σ and are smaller than the symbols when not shown. Note that the early-stage granitoids are systematically higher in Nb-Ta concentrations and (Gd/Lu)_N ratios than the late-stage granitoids.

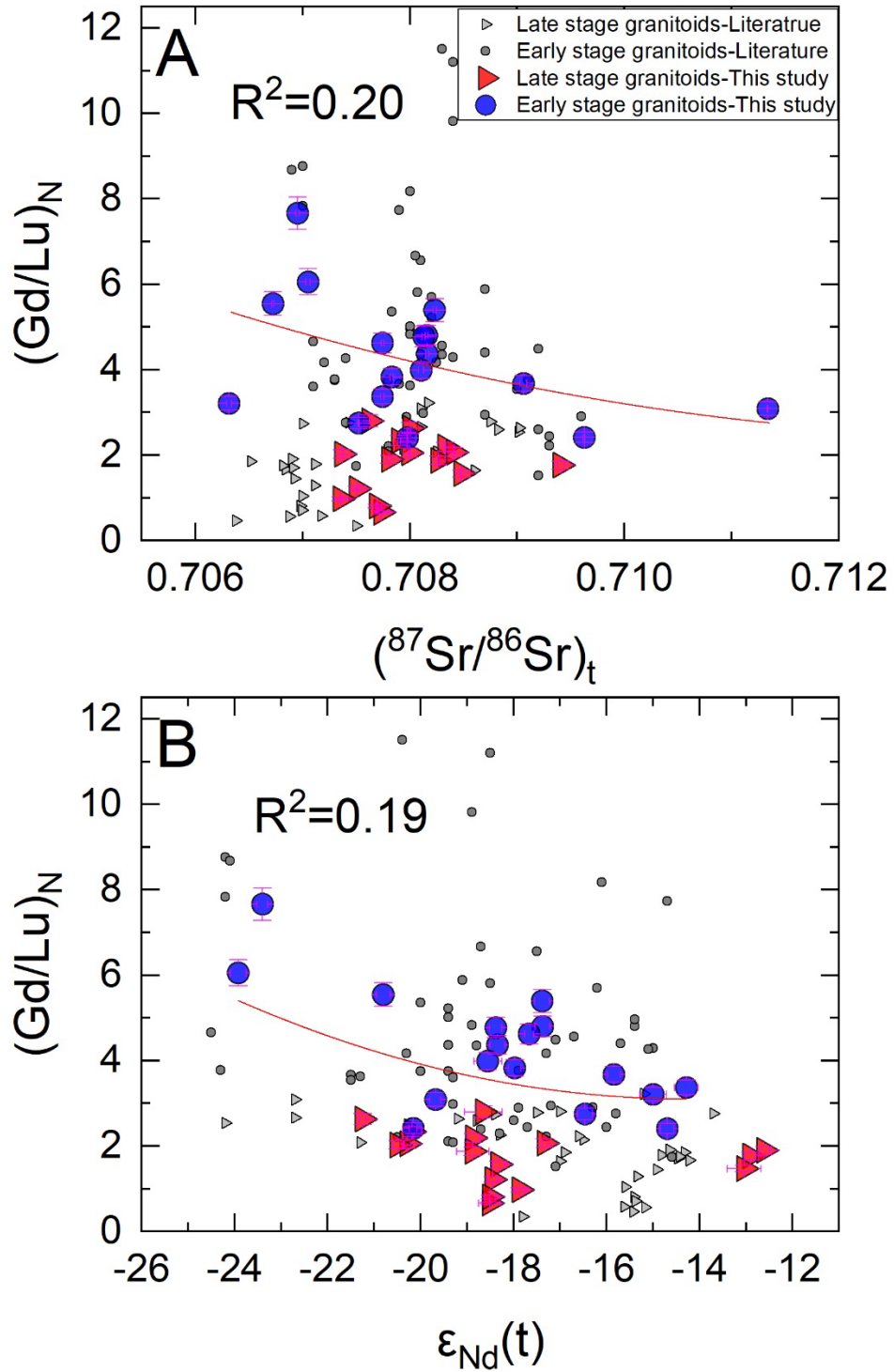


Figure S5. Plots of $(^{87}\text{Sr}/^{86}\text{Sr})_t$ (A) and $\epsilon_{\text{Nd}}(t)$ (B) versus $(\text{Gd}/\text{Lu})_N$ ratios for the post-collisional early-stage and late-stage granitoids from the Dabie orogen, published data (Zhao et al., 2017) are also plot for comparison. Uncertainties are plotted at 2σ and are smaller than the symbols when not shown. Note that the covariation between $(^{87}\text{Sr}/^{86}\text{Sr})_t$ or $\epsilon_{\text{Nd}}(t)$ and $(\text{Gd}/\text{Lu})_N$ ratio is much weaker than this between $\epsilon_{\text{Hf}}(t)$ and $(\text{Gd}/\text{Lu})_N$ ratio.

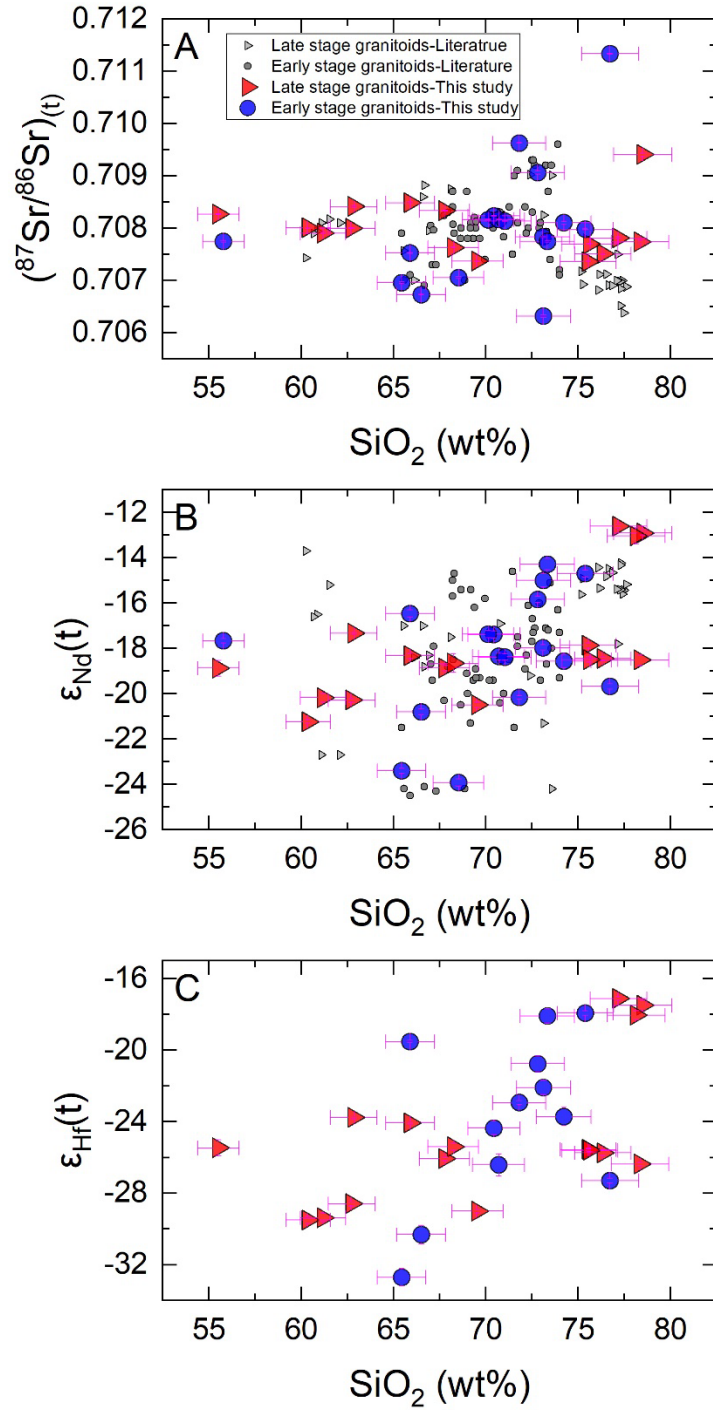


Figure S6. Plots of $(^{87}\text{Sr}/^{86}\text{Sr})_t$ (A), $\epsilon_{\text{Nd}}(t)$ (B), and $\epsilon_{\text{Hf}}(t)$ (C) versus SiO_2 values for the post-collisional early-stage and late-stage granitoids from the Dabie orogen, published data (Zhao et al., 2017) are also plot for comparison. Note that there is a lack of visible covariation between isotope compositions and SiO_2 contents for both early-stage and late-stage granitoids.

Part IV: Details for quantitative simulation

Our qualitative analyses suggest that different amounts of garnet residue during partial melting, or entrainment of different amounts of garnet rich in radiogenic Hf during melt segregation, could produce the observed covariation patterns between whole-rock Hf isotope and HREE fractionation. We tested these two models by carrying out quantitative modeling to simulate the Hf isotope and (Gd/Lu)_N ratio variations in the magmas/granitoids.

As stated in the text, the Triassic-formed eclogitic mafic rocks in the Dabie orogen are documented to be the primary source rocks of the early-stage granitoids. Therefore, we calculated the Hf isotope evolution of the Triassic eclogites in the Dabie orogen and garnet grains within them as a function of time from ~230 Ma when eclogitic rocks and thus most garnet formed, to ~130 Ma when anatexis of these eclogitic rocks and thus garnet effect occurred. The initial Hf isotope composition and Lu/Hf ratios for the eclogites and garnet grains at 230 Ma were adopted from [Cheng et al. \(2008, 2009\)](#), and are listed in [Table S5](#). It's noteworthy that two sets of whole-rock compositions for the eclogites that obtained from (1) the bomb-digestion technique, by which all zircon would be dissolved and thus release all the Hf, and (2) the Savilex-digestion technique, by which minimal, if any zircon would be dissolved ([Table S6](#); [Cheng et al., 2008, 2009](#)). According to the difference in whole-rock Hf concentrations obtained using the aforementioned two techniques, and the proportion (~40 wt.%; estimated from [Cheng et al., 2008, 2009](#)) and Hf concentration for the garnet in the eclogites ([Table S11](#)). Zircon and garnet have contributed ~81% and ~3% of the total Hf budget in the Dabie eclogites, respectively ([Table S12](#)). However, if most zircon Hf was inactive during crustal anatexis as suggested by many studies ([Farina et al., 2014](#); [Tang et al., 2014](#); [Chen et al., 2015](#); [Zhang et al., 2020](#); [Gao et al., 2022](#)), garnet would contribute up to 23% of Hf budget in the system ([Table S11](#)).

The Gd, Lu, and Hf concentrations of the residual garnet are adopted from the Dabie eclogites ([Cheng et al., 2008, 2009](#)), and the Hf isotope composition of these garnets is calculated at 130 Ma ([Table S6](#)). Since the garnet did not participate in the melting reaction, the effective bulk composition of the eclogitic rocks underwent partial melting ([Table S6](#)) and was calculated by removing the

garnet component from the four eclogitic samples ([Bomb-digested bulk compositions of Cheng et al., 2008, 2009](#)) using the garnet composition adopted from Garnet-2 in sample TH12 of [Cheng et al.\(2009\)](#)—the only garnet grain that all the necessary data including Lu, Hf, Gd, and $^{176}\text{Hf}/^{177}\text{Hf}$ values is available ([Table S6](#))—and residual garnet proportion according to Run 3124 of [Qian and Hermann \(2013\)](#). Unfortunately, Gd values for the eclogite whole rocks were not reported for the selected four eclogites in the original papers of [Cheng et al. \(2008, 2009\)](#). Therefore, the unpublished Gd value of 0.90 from Triassic eclogites sample 09DB30 from the Shuanghe area in the Dabie orogen that was kindly shared by Prof. Xiaoying Gao from the University of Science and Technology of China was assigned for these eclogites ([Table S6](#)). The peritectic garnets Hf isotope compositions should be the same as that of the anatectic melts, and their HREE contents can be calculated using the bulk trace element partitioning coefficients between garnet, melt, and sources ([Table S8](#); [Run 3124 of Qian and Hermann, 2013](#)), as well as the effective bulk composition of the eclogitic rocks undergoing partial melting ([Table S6](#)). Due to the sequestration of radiogenic Hf and the HREE in the residual garnet during disequilibrium melting, peritectic garnet is poor in radiogenic Hf and strongly depleted in HREE relative to the general residuum ([Table S8](#)).

Once all the parameters are selected, residual garnets were then added into granitoid sample 15DB141—which has the highest $(\text{Gd}/\text{Lu})_{\text{N}}$ value and, therefore, interpreted to be the closest approximation to initial melt with the least garnet entrainment—to calculate the compositions of the anatectic melts produced by garnet entrainment using the binary mixing function of [Langmuir et al. \(1978\)](#). The mass percent of each end member is set to vary from 0 to 1 with varying steps ([Table S9](#)). Mixing generates values that are either low in $(\text{Gd}/\text{Lu})_{\text{N}}$ ratios or decrease in $(\text{Gd}/\text{Lu})_{\text{N}}$ with minimal change in melt $\varepsilon_{\text{Hf}}(t)$ ([Table S9](#)); these values are inconsistent with that of early granitoids ([Fig. 3D](#)).

Besides residual garnet, peritectic garnet would also be entrainment ([Stevens et al., 2007](#)). The peritectic garnets Hf isotope compositions should be the same as that of the anatectic melts, and their HREE contents can be calculated using the bulk trace element partitioning coefficients between garnet, melt, and sources ([Tables S7 and S8](#)), as well as the effective bulk composition

of the eclogitic rocks undergoing partial melting (Table S6). Due to the sequestration of radiogenic Hf and the HREE in the residual garnet during disequilibrium melting, peritectic garnet is poor in radiogenic Hf and strongly depleted in HREE relative to the general residuum (Table S8). Adding peritectic garnet to the melts decreased the $(\text{Gd}/\text{Lu})_N$ value of the melts at consistent $\epsilon_{\text{Hf}}(t)$ (Table S10), which also cannot explain the observed covariation trend (Fig. 3D).

In the scenario of disequilibrium melting and residual garnet, the parental melts of the early granitoids could be mixtures of melts derived from sources with variable modal contents of garnet, which is observed in the Dabie-Sulu eclogites (Feng et al., 2021). We account for this by binary mixing of granitoid sample 15DB141 and partial melts of the garnet-poor sources (Table S6). The former shows the highest $(\text{Gd}/\text{Lu})_N$ value and may represent the partial melt of a source with the most residual garnet, and the latter represent melts derived from sources with the least residual garnet (negligible garnet effect). As stated above, the anatectic melt compositions (Table S7) from garnet-poor sources are calculated using the bulk trace element partitioning coefficients between melt and source (Run 3124 of Qian and Hermann, 2013), and the effective bulk composition of the eclogitic rocks (Table S6) that undergoing partial melting. The mixing is calculated using the binary mixing function of Langmuir et al. (1978), the mass percent of each end member is set to vary from 0 to 1 with a step of 0.1, and the results are listed in Table S11. The resulting mixing trends passed nearly all of the early granitoids but very few of the late granitoids (Figs. 3D). This confirms the inference that mixing between melts produced by the anatexis of metamafic sources containing different amounts of residual garnet controls the covariation between $(\text{Gd}/\text{Lu})_N$ and $\epsilon_{\text{Hf}}(t)$ of the early granitoids and did not influence the late granitoids.

Although the possible inadequate representation of the protolith by the four eclogite samples, the likely contribution of crustal rocks other than the subducted SCB mafic rocks to the source of the granitoids (He et al., 2011; Zhao et al., 2017), the limit compositional data for garnet from the eclogites, as well as possible zircon effect, would introduce some uncertainties, our garnet residual modeling results perfectly reproduced the measured values and covariation patterns for the early granitoids in the Dabie Orogen. Consequently, the role of residual garnet on the Hf isotope composition of granitoids may be

an underappreciated process when linking sources to sinks and in understanding the long-term evolution of the continental crust based on the whole-rock and zircon Hf isotope archive.

Part V: Captions for supplemental tables S1-S11

Table S1. Selected published whole-rock major and trace elements data for the post-collisional late-stage granitoids from the Dabie orogen that was used for Sr-Nd-Hf isotope analysis and comparative study.

Table S2. LA-ICPMS zircon U-Th-Pb isotopes data for the post-collisional early-stage granitoids from the Dabie orogen.

Table S3. Whole-rock major and trace element data for the post-collisional early-stage granitoids from the Dabie orogen.

Table S4. Whole-rock Rb-Sr, Sm-Nd, and Lu-Hf isotopes data for the post-collisional early-stage and late-stage granitoids from the Dabie orogen.

Table S5. Parameters used in whole-rock and garnet Hf isotope ingrowth calculation in **Figure 3C**.

Table S6. The reported composition for the Dabie eclogites and garnet within them, and the effective bulk composition of these eclogites that underwent partial melting.

Table S7. Bulk partitioning coefficients between melt and eclogitic rock and the composition of anatectic melts from the Dabie eclogites.

Table S8. The composition of peritectic garnets produced by the partial melting reaction of the Dabie eclogites that calculated using bulk partitioning coefficients between garnet and melt.

Table S9. Table S9. Modeling results for residual garnet entrainment.

Table S10. Table S10. Modeling results for peritectic garnet entrainment.

Table S11. Modeling results for mixing between melts derived from garnet-poor and garnet-rich residuum.

Table S12. Zircon and garnet Hf budgets in the Dabie eclogites.

References cited in the supplemental materials:

Bouvier, A., Vervoort, J.D., Patchett, P.J., 2008. The Lu-Hf and Sm-Nd isotopic composition of CHUR: constraints from unequilibrated chondrites and implications for the bulk composition of terrestrial planets. *Earth and Planetary Science Letters* 273, 48-57.

Cheng, H., King, R. L., Nakamura, E., Vervoort, J. D., and Zhou, Z., 2008, Coupled Lu–Hf and Sm–Nd geochronology constrains garnet growth in ultra - high - pressure eclogites from the Dabie orogen: *Journal of Metamorphic Geology*, v. 26(7), p. 741-758, <https://doi.org/10.1111/j.1525-1314.2008.00785.x>

Cheng, H., Nakamura, E., and Zhou, Z., 2009, Garnet Lu–Hf dating of retrograde fluid activity during ultrahigh-pressure metamorphic eclogites exhumation: *Mineralogy and Petrology*, v. 95(3-4), p. 315-326, <https://doi.org/10.1007/s00710-008-0030-5>.

Feng, P., Wang, L., Brown, M., Johnson, T. E., Kylander-Clark, A., and Piccoli, P. M., 2021, Partial melting of ultrahigh-pressure eclogite by omphacite-breakdown facilitates exhumation of deeply-subducted crust: *Earth and Planetary Science Letters*, v. 554, 116664, <https://doi.org/10.1016/j.epsl.2020.116664>.

He, Y., Li, S., Hoefs, J., Huang, F., Liu, S. A., and Hou, Z., 2011, Post-collisional granitoids from the Dabie orogen: new evidence for partial melting of a thickened continental crust: *Geochimica et Cosmochimica Acta*, v. 75(13), p. 3815-3838, <https://doi.org/10.1016/j.gca.2011.04.011>.

Langmuir C. H., Vocke R. D., Hanson G. N., & Hart S. R. (1978), A general

- mixing equation with applications to Icelandic basalts. *Earth and Planetary Science Letters*, 37, 380-392. [https://doi.org/10.1016/0012-821X\(78\)90053-5](https://doi.org/10.1016/0012-821X(78)90053-5).
- Münker, C., Weyer, S., Scherer, E., Mezger, K., 2001. Separation of high field strength elements (Nb, Ta, Zr, Hf) and Lu from rock samples for MC-ICPMS measurements. *Geochemistry, Geophysics, Geosystems* 2 (12), doi: 10.1029/2001GC00001.
- Nebel, O., Scherer, E.E., Mezger, K., 2011. Evaluation of the ^{87}Rb decay constant by age comparison against the U-Pb system. *Earth and Planetary Science Letters* 301, 1-8.
- Pin, C., Zalduegui, J. S., 1997. Sequential separation of light rare-earth elements, thorium and uranium by miniaturized extraction chromatography: application to isotopic analyses of silicate rocks. *Analytica Chimica Acta*, 339(1), 79-89.
- Scherer, E., Münker, C., Mezger, K., 2001. Calibration of the lutetium-hafnium clock. *Science* 293, 683-687.
- Wu, F.-Y., Yang, Y.-H., Xie, L.-W., Yang, J.-H. Xu, P., 2006. Hf isotopic compositions of the standard zircons and baddeleyites used in U-Pb geochronology. *Chemical Geology* 234, 105-126.
- Yang, Y. H., Wu, F. Y., Wilde, S. A., Liu, X. M., Zhang, Y. B., Xie, L. W., Yang, J. H., 2009. In situ perovskite Sr–Nd isotopic constraints on the petrogenesis of the Ordovician Mengyin kimberlites in the North China Craton. *Chemical Geology* 264, 24-42.
- Yang, Y.H., Zhang, H.F., Chu, Z.Y., Xie, L.W., Wu, F.Y., 2010. Combined chemical separation of Lu, Hf, Rb, Sr, Sm and Nd from a single rock digest and precise and accurate isotope determinations of Lu-Hf, Rb-Sr and Sm-Nd isotope systems using Multi-Collector ICP-MS and TIMS. *International Journal of Mass Spectrometry* 290, 120-1.
- Yuan, H.-L., Gao, S., Liu, X.-M., Li, H.-M., Gunther, D., Wu, F.-Y., 2004. Accurate U–Pb age and trace element determinations of zircon by laser ablation-inductively coupled plasma mass spectrometry. *Geostand Newsletter* 28, 353–370.
- Zhao, Z.-F., Liu, Z.-B., and Chen, Q., 2017, Melting of subducted continental crust: Geochemical evidence from Mesozoic granitoids in the Dabie-Sulu

orogenic belt, east-central China: *Journal of Asian Earth Sciences*,
<https://doi.org/10.1016/j.jseaes.2017.03.038>.

Zong, K.Q., Liu, Y.S., Gao, C.G., Hu, Z.H., Gao, S., Gong, H.J., 2010. In situ U–Pb dating and trace element analysis of zircons in thin sections of eclogite: refining constraints on the UHP metamorphism of the Sulu terrane, China. *Chemical Geology* 269, 237-251.